**********Newcastle Univeristy EPRINT version**********
**********Originally presented at PEMD 2018 - will be available on IEEE XPLORE late 2018**********
**********The 9th International Conference on Power Electronics, Machines and Drives (IET)**********

A study of the assembly, build and test of a linear transverse flux machine

J. Wang*, N.J. Baker*, B. Gavrilov*

** Electrical Power Group, School of Electrical Engineering, Newcastle University, UK, NE17RU,*

Keywords: Linear machine, transverse flux, free piston engine, finite element analysis

Abstract

This paper discusses the topology development of a cylindrical transverse flux linear machine for use with a free piston engine. Despite its three dimensional flux path, the stator of this topology can be made from regular laminated components and only the translator includes soft magnetic composites.

The detailed design development is discussed, including stator tooth combination, alternative winding and fabrication techniques. Results from both finite element analysis and experimental measurement are compared, which gives a validation of the feasibility of the building process.

1 Introduction

The transverse flux machine (TFM) is attractive to designers who are working on high torque or thrust applications [1]. The high force density is mainly due to the decoupling property that electric loading and magnetic loading can be separately designed [2]. The 3D flux flow often requires the use of soft magnetic composites (SMC) to guide the flux around the stator winding. Machine building and assembly also poses challenges compared to other linear machines which can be built from flat laminations in the conventional manner. Rotary versions of the TFM have been presented using SMC [3], flat laminations [4], a combination of smc and flat laminations [5-6] and bent laminations [6]. The advantage of having no competition between space requirements of flux carrying teeth and space occupied by windings is well documented in [7].

In previous studies [8-10] linear TFMs have been compared with more conventional longitudinal topologies for use with a Free-Piston Engine. Simulation results show that a modulated pole machine (MPM) type TFM topology can achieve high force, low copper loss and competitive power factor even under conditions of high electric loading. However, the assembly, building and testing problems are still unsolved. In this paper the authors will perform a detailed design and testing of the linear MPM as a special linear machine prototype.

2 Initial machine topology

The initial machine topology based on previous studies [10] is as shown in Figure 1, where the translator has axially magnetised permanent magnets separated by iron pole pieces, the stator consists of three separate phases, each with a set of iron teeth surrounding the copper coil. Each phase covers 120 mechanical degrees around the circumference of the translator. Arrows illustrate the flux concentration from the inner radius of coupled magnets on the translator part. At the peak mutual flux position (a), flux are concentrated in the pole piece and flows into the stator teeth, where it encompasses the coil and returns to the translator by an adjacent tooth. In position (b), the flux is shorted by the stator tooth, and so the equivalent flux encompassing the coil is 0. An overall three phased topology with elongated translator is presented in (c).

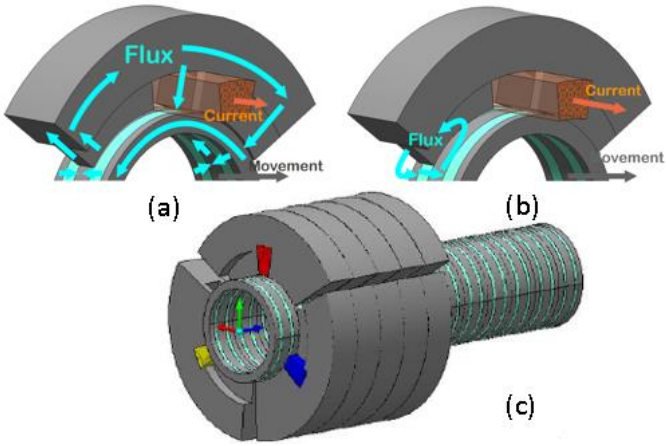

Figure 1 Initial topology (a) Single phase peak flux path
(b) Single phase 0 flux path (c) Three phase machine

3 Topology development

Based on the initial topology (MPM), which showed promise for the Free Piston engine, a more detailed design study of the topology has been carried out to consider development of the stator tooth shape, the winding and the stator lamination fabrication. By completing a series of developments, detailed below, a simpler construction, higher efficiency and lower material cost design has been achieved.

3.1 Stator topology development

Figure 2 gives an evolutionary process of a single pole paired topology. Starting from the baseline separated stator topology as shown in (a), there are three SMC core backs and six individual lamination teeth. Figure 2 (b) shows the fully pitched stator teeth as presented, where teeth from adjacent phases are in physical contact. Adjacent phase teeth can be combined, forming a "combined phase machine" as shown in figure 2 (c), which now only requires three individual lamination teeth, similar to its rotary counterpart [11]. A more direct view in 2-D version is presented in Figure 3, it can be observed that this tooth combination process does not influence any material usage but only reduces the overall assembly difficulty. Topologies are modelled in 3D electromagnetic finite element analysis to investigate topology developments. Force profiles are presented in Figure 4, it can be observed that the tooth combination process can not only recover the force reduction (6%) in full pitched model but can also boost the force to 6% more. Moreover, such a change in the stator tooth can effectively reduce the number of building components without changing the phase EMF harmonics.

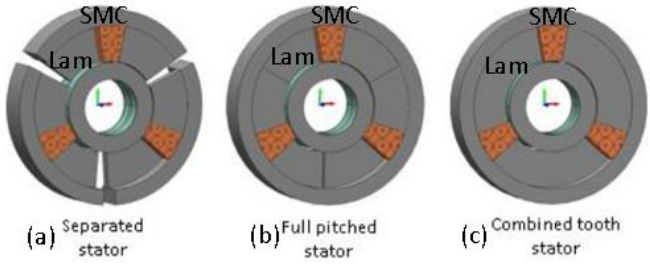

Figure 2 Stator topology development (a) Baseline separated stator, (b) Full pitched stator (c) Combined tooth stator

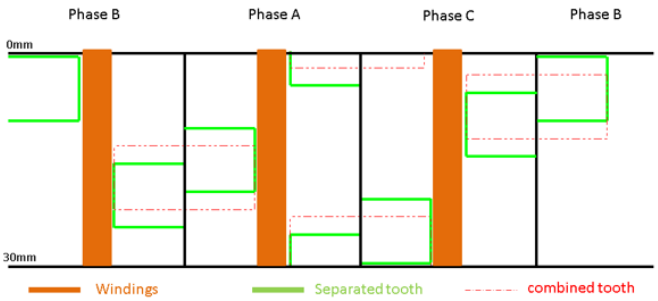

Figure 3 2D sketch diagram of the topology development

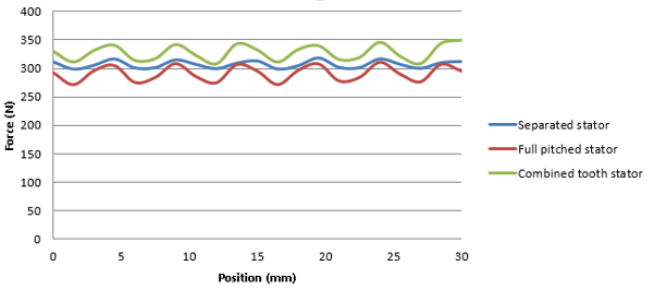

Figure 4 Force profile along the topology development

3.2 Winding development

In all these three topologies, the return path of the coil is on the outer surface of the stator as presented in Figure 5(a). By switching to a single toothed type winding as shown in Figure 5(b), the copper usage can be improved and winding can be simplified. In theory, applying such a winding topology can effectively reduce the copper usage to 50% (ignoring end windings). However, a drawback of this is the force reduction due to the low winding factor. If machine dimensions and current density are all maintained with the same coil cross section, then the phase MMF of the single tooth winding will reduce to half of that in (a), meanwhile both out and return coils are contributing to the machine force output. However such winding topology was found to give a 23% force reduction in simulations due to the short pitch factor (k_p) between out and return sides of the coils.

Figure 6 shows a phasor diagram of the single tooth winding machine. Vectors *ab* and *bc* represent the phase of the flux linking the out and return windings respectively and *ac* represents the vector sum. From calculation k_p is 0.866 which matches well the 23% reduction in force observed. Such force reduction can simply be redeemed by increasing the phase MMF in the single tooth winding. The final topology shows that it is possible to recuperate the force by increasing the coil area and electric loading whilst still achieving 37% less copper loss compared to the combined tooth topology with the original windings (force profiles are summarised in Figure 7). What is more, by using the single tooth winding topology the total harmonic distortion of EMF harmonics can be improved by 50%.

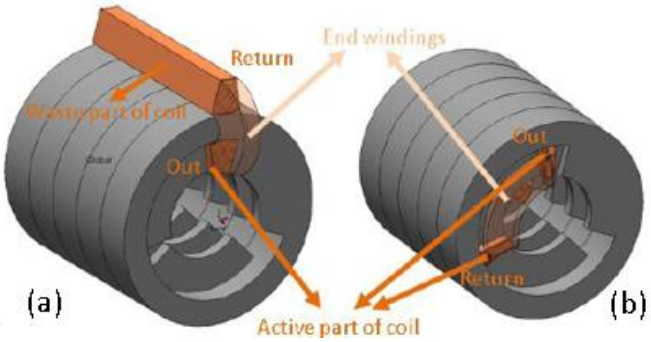

Figure 5 Windings development (a) Return path outside of the machine (b) Returned end winding single tooth type winding

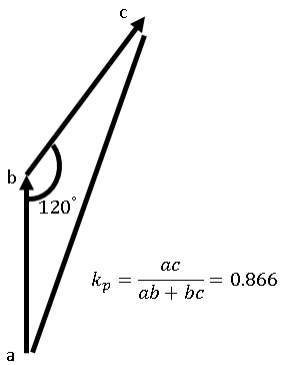

Figure 6 Phasor diagram of the winding factor

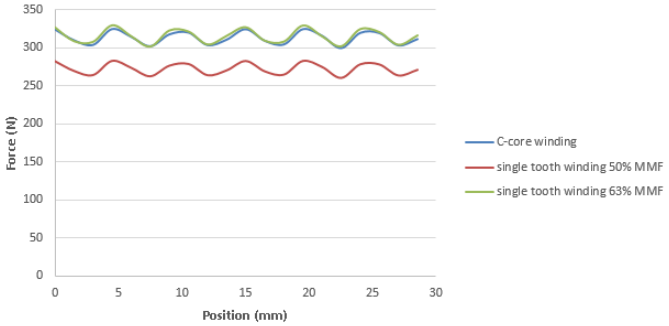

Figure 7 Force profile along the winding development

3.3 Lamination development

Four alternative construction options are shown in Figure 8, aiming to reduce reliance on SMC material in the stator. In (a), stator teeth are composed of steel laminations, where the flux is radial, and an SMC core back ring is used to allow flux flow in the circumferential and axial directions. Figure 8(b) extends the tooth lamination area and replaces the SMC ring with smaller SMC blocks. In (c), a further minimization of the SMC block to a smaller square cross section is shown. In this case, flux flow in the SMC is primarily in the axial and circumferential direction. In (d) the SMC is replaced by a radially laminated block. In this case, the stator teeth provide a 2D flux path in the (x, y) plane whereas the radially laminated block provides a 2D flux path in the (x, z) plane. Thus a 3D flux path can be formed without the use of SMC. The simulated performance of the four machines are shown in Figure 9, where it can be seen that the SMC free option (d) has 96% of the flux flow and develops 92% of the force of the SMC version.

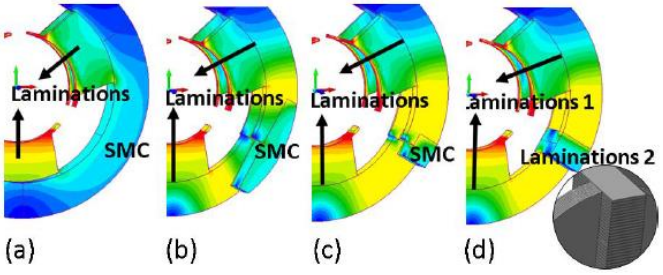

Figure 8 Lamination development

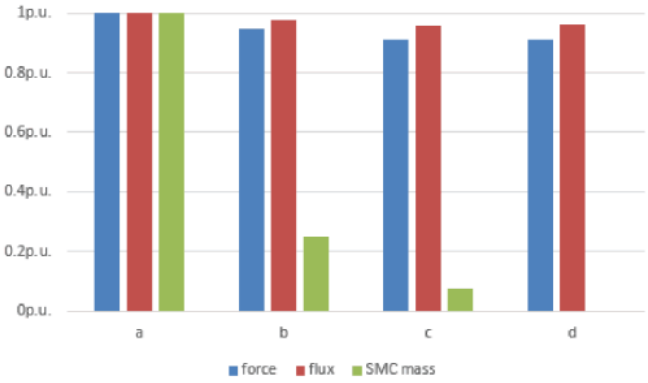

Figure 9 Performance comparison

4 Prototype building

In this section, detailed building processes of the developed MPM will be presented including the translator build, the stator build and the winding build.

4.1 Translator building

The active part of the translator is composed of SMC pole pieces and axially magnetised magnets. In addition, the translator is also composed of the translator support, two end caps and two shafts. The general layout is as presented in Figure 10. Mechanical FEA simulations are used to estimate the required shaft dimension to counter the translator deformation using just

static loads. The deformation of the translator could not only influence the effective air gap length and thus effect the machine performance, but could also damage the magnet and thus destroy the machine.

A side load magnetic force is produced due to asymmetry of the three phase stator teeth structure. There is ripple variation in the resultant amplitude and the resultant direction effectively rotates with the translator position. In other words, if it is assumed that the magnetic cogging and force are produced along the z axis then the side load is produced at the plane along x and y axis in a rotating form.

Results from the simulation indicate that peak no load side load is 500N and the peak on load side load is about 1750N. For the worst case scenario, the peak on load side load could align to the gravity. The resultant translator deflection varies with translator position, and two extreme positions are considered in Figure 11. The final dimensions of the translator (25mm shaft diameter and 20mm male thread diameter) and its estimated deformation are presented in Figure 12.

It can be concluded that by selecting these dimensions, the biggest deformation will be no more than 0.1 mm with a good safety factor of three, where most designers strive for a safety factor of between two to four based on the highest expected load scenario [12]. The final assembled translator is presented in Figure 13.

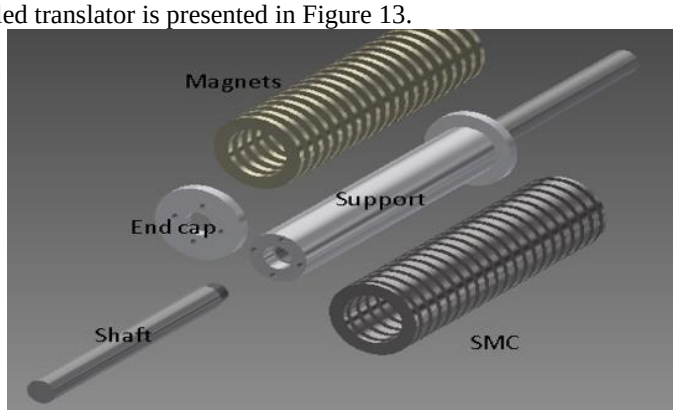

Figure 10 General translator layout

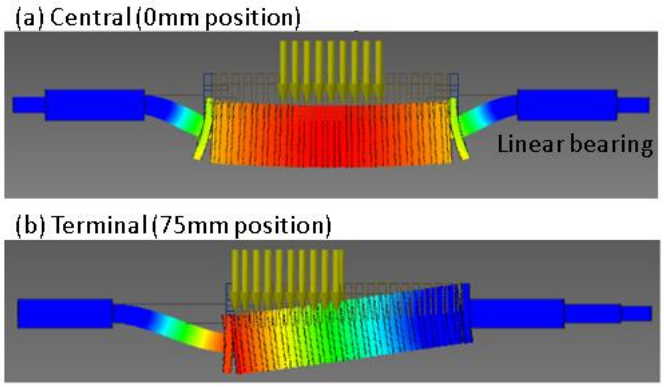

Figure 11 Deformations based on two extreme positions

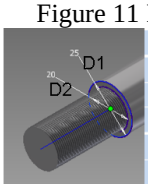

Position (mm) with load	Max deformation (mm)	Min safety factor
0	0.03143	4.88
75	0.09638	2.96
Position (mm) no load	**Max deformation (mm)**	**Min safety factor**
0	0.01004	15
75	0.0297	9.63

Figure 12 Final deformations with 25mm shaft diameter and 20mm male thread diameter

Figure 13 Assembled translator

4.2 Stator building

The stator laminated components are shown in Figure 14(a). A rapid prototyping 3D printed support was formed to contain lamination components as shown in Figure 14(b). The assembled support and laminations are as shown in Figure 15.

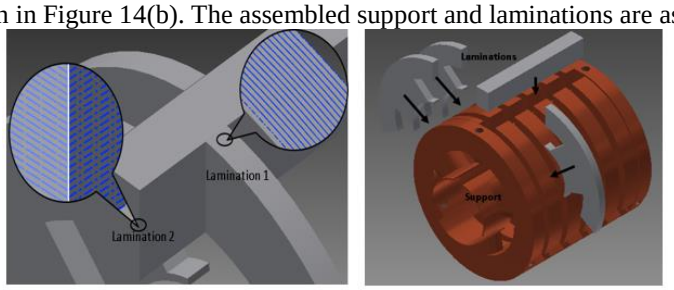

(a) Laminations sketch (b) 3D printing support and laminations

Figure 14 Laminations and support sketch

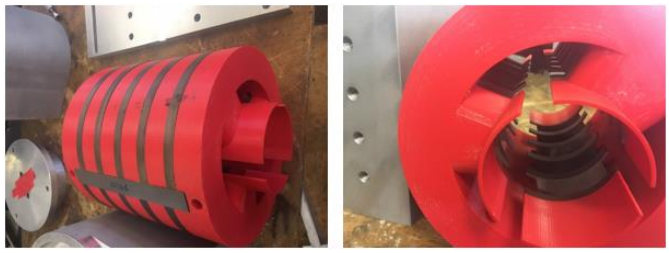

(a). Outer view (b). Inner view

Figure 15 Assembled laminations and support

4.3 Winding building

In practise, manual winding of the machine could only achieve a fill factor of around 0.3, due to the bend ratio of end windings. To achieve a higher fill factor, an elongated 3D printed bobbin was designed, Figure 16 (a), and mounted in a lathe, Figure 16 (b). The completed winding, Figure 17(a), is relocated to the stator assembly in Figure 17(b). By this winding process, a fill factor of 0.53 was achieved.

(a). Bobbin unit model (b). Winder machine

Figure 16 Bobbin and winder

(a). Windings removed from the bobbin (b). Windings relocated to the stator support

Figure 17 Windings relocation

5 Prototype testing and modelling

5.1 Test rig

The machine was tested using a ball screw as shown in Figure 18.

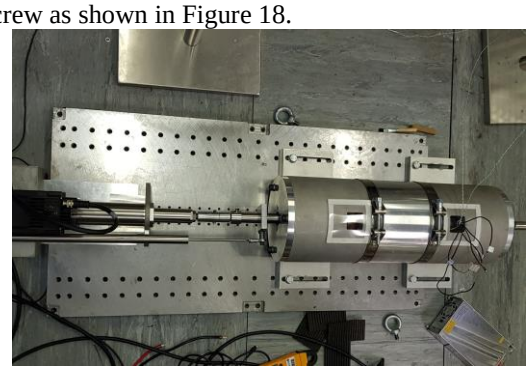

Figure 18: TFM linear test rig.

5.2 Predicted results (ideal Simulation)

Finite Element Analysis (FEA) open circuit emf predictions of the ideal machine are shown in Figure 19 (a) for an oscillation of 100 mm with a peak velocity of 50 mm/s. EMF induced in all three coils is identical with peak of 0.6 V per phase during peak translator velocity.

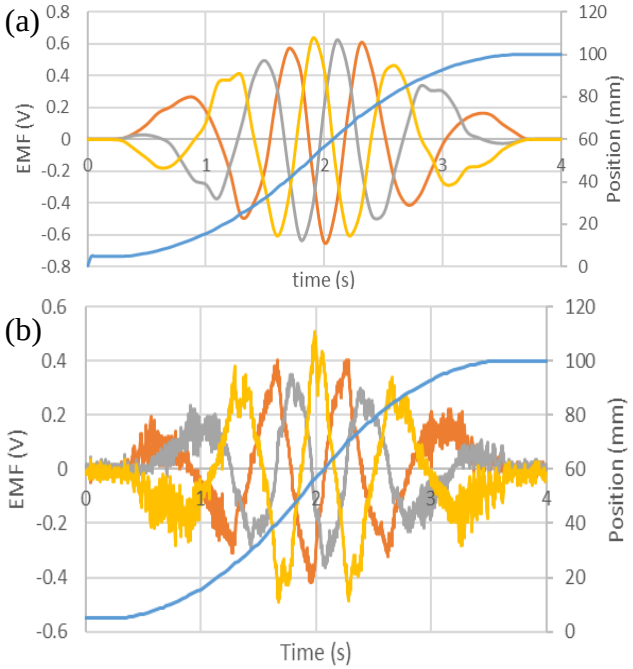

Figure 19: Simulated (a) and experimental (b) low speed test back emf

The equivalent experimental results are shown in Figure 19 (b), with the peak EMF being between 0.43 V and 0.4 V in different phases. The discrepancy is close to 28%, which is attributed to parasitic air gaps within the machine. In-balance between phases is assumed to be as a result of translator eccentricity. Both these effects are investigated below.

5.3 Parasitic airgaps

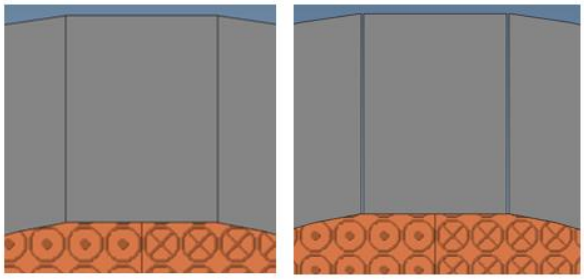

Figure 20: parasitic air gaps between components.

The separate components of the stator are slotted together and held in a 3D printed plastic holder. This was found to give rise to parasitic airgaps between the laminated teeth and bars, visible in Figure 15 (a). To account for this, the FEA model was adapted as shown in Figure 20 to include air gaps between 0.1 and 0.3 mm. Simulation results are shown in Figure 21 and rms values in Table 1.

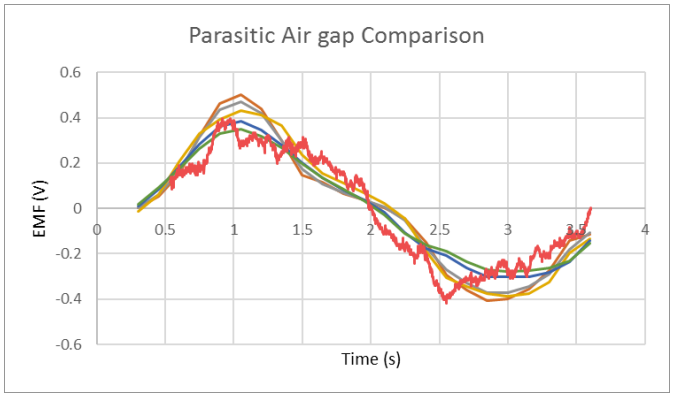

Figure 21: Parasitic air gap comparison to real TFM performance.

	Simulated gap size (mm)					Experimental
	0	0.1	0.15	0.2	0.3	
emf (V_{rms})	0.273	0.263	0.275	0.233	0.217	0.233

Table 1: RMS open circuit emf values over positive cycle

From this crude study, it appears an average gap of 0.2 mm exists between laminated stator components.

5.4 Translator offset (modified simulation)

When the machine is assembled, the stator casing prevents measurement of the physical airgap. Although tolerance on the magnets and SMC components was good, and predicted shaft deflection is less than 0.1 mm, the results imply the translator is not concentric with the stator. To understand how translator offset affects machine performance, the transient simulation was run with a translator offset, assuming a shift equally towards one of the coils and equally away from the other two. RMS values of flux linkage varies less than 2% across the 3 coils in the perfectly centred machine, whereas an offset of 0.5 mm gave a difference of 16% between phases.

5.5 Validating results

A second set of experimental results is used to validate the modified FEA model which includes the 0.2 mm offset and the 0.1 mm parasitic airgaps. The rig was run with a maximum velocity of 300 mm/s and experimental and simulated results are shown in Figure 22. The maximum simulated peak EMF across the three phases is 3.13 V, 2.8 V and 2.3 V. The equivalent experimental results are 2.95 V, 2.5 V and 2.0 V, implying a simulation error of 6-15%.

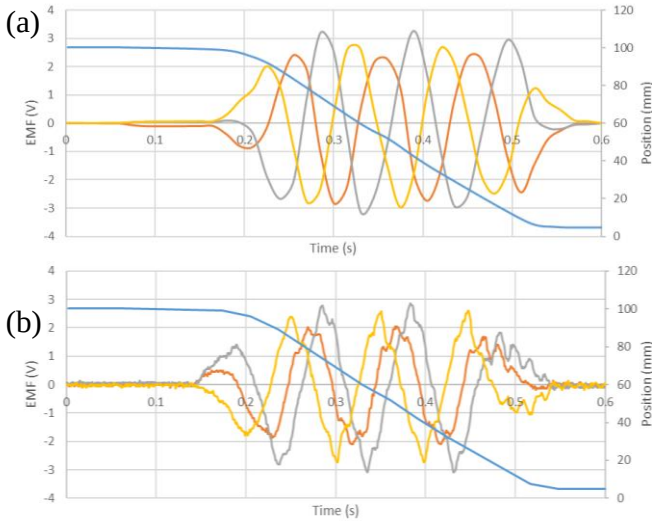

Figure 22: Simulated (a) and experimental (b) high speed test back emf, using modified FEA model to account for airgaps and offset translator. (One of the experimental phases requires inverting)

6 Conclusion

A cylindrical transverse flux linear machine has been developed, analysed and built. A combined phase, single tooth wound stator is made from segmented laminated steel and surrounds a translator made from soft magnetic composite and permanent magnets. Details of the prototype build process including translator deformation, stator lamination assembly and winding assembly are performed.

Experimental results have been presented, including a study on the translator offset and parasitic airgaps. It is estimated that gaps of around 0.2 mm exist between segments.

References

[1] Anglada, J.R. and Sharkh, S.M., 2017. Analysis of Transverse Flux Machines using a Virtual Mutual Inductance Approach. *IEEE Transactions on Energy Conversion*.

[2] Hasanien, H.M., Abd-Rabou, A.S. and Sakr, S.M., 2010. Design optimization of transverse flux linear motor for weight reduction and performance improvement using response surface methodology and genetic algorithms. *IEEE Transactions on Energy Conversion*, *25*(3), pp.598-605.

[3] Lei, G., Liu, C., Guo, Y. and Zhu, J., 2015. Multidisciplinary design analysis and optimization of a PM transverse flux machine with soft magnetic composite core. *IEEE Transactions on Magnetics*, *51*(11), pp.1-4.

[4] Lu, K. and Wu, W., 2015. High Torque Density Transverse Flux Machine Without the Need to Use SMC Material for 3-D Flux Paths. *IEEE Transactions on Magnetics*, *51*(3), pp.1-4.

[5] Washington, J.G., Atkinson, G.J., Baker, N.J., Jack, A.G., Mecrow, B.C., Jensen, B.B., Pennander, L.O., Nord, G.L. and Sjöberg, L., 2012. Three-phase modulated pole machine topologies utilizing mutual flux paths. *IEEE Transactions on Energy Conversion*, *27*(2), pp.507-515.

[6] S. Jordan and N. Baker, "Comparison of Two Transverse Flux Machines for an Aerospace Application" *IEEE Int Electric Machines and Drives Conf* (IEMDC). 2017, Miami, FL, USA

[7] Hasanien, H.M., Abd-Rabou, A.S. and Sakr, S.M., 2010. Design optimization of transverse flux linear motor for weight reduction and performance improvement using response surface methodology and genetic algorithms. *IEEE Transactions on Energy Conversion*, *25*(3), pp.598-605.

[8] Wang, J. and Baker, N.J., 2015, May. Comparison of flux switching and modulated pole linear machines for use with a free piston. In *Electric Machines & Drives Conference (IEMDC), 2015 IEEE International* (pp. 642-648). IEEE.

[9] Wang, J. and Baker, N.J., 2016. A comparison of alternative linear machines for use with a direct drive free piston engine. 8th IET International Conference on Power Electronics, Machines and Drives (PEMD 2016)

[10] Baker, N.J., Wang, J. and Atkinson, G.J., 2016, September. Optimization and comparison of linear transverse flux and flux switching machines. In *Electrical Machines (ICEM), 2016 XXII International Conference on* (pp. 2471-2477). IEEE.

[11] Washington, J.G., Atkinson, G.J., Baker, N.J., Jack, A.G., Mecrow, B.C., Jensen, B.B., Pennander, L.O., Nord, G.L. and Sjöberg, L., 2012. Three-phase modulated pole machine topologies utilizing mutual flux paths. *IEEE Transactions on Energy Conversion*, *27*(2), pp.507-515.

[12] Zhao, S., Zheng, Y.R., Shi, W. and Wang, J.L., 2002. Analysis on safety factor of slope by strength reduction FEM. *CHINESE JOURNAL OF GEOTECHNICAL ENGINEERING-CHINESE EDITION-*, *24*(3), pp.343-346.